Chinese Journal of Chemical Engineering 53 (2023) 346–360

Contents lists available at ScienceDirect

Chinese Journal of Chemical Engineering

journal homepage: www.elsevier.com/locate/CJChE

Full Length Article

Process analysis of temperature swing adsorption and temperature vacuum swing adsorption in VOCs recovery from activated carbon

Yadong Li, Yuanhui Shen, Zhaoyang Niu, Junpeng Tian, Donghui Zhang *, Zhongli Tang, Wenbin Li

Collaborative Innovation Center of Chemical Science and Engineering, The Research Center of Chemical Engineering, School of Chemical Engineering and Technology, Tianjin University, Tianjin 300072, China

ARTICLE INFO

Article history:
Received 5 September 2021
Received in revised form 15 January 2022
Accepted 24 January 2022
Available online 22 March 2022

Keywords:
VOCs
TSA
TVSA
Activated carbon
Benzene

ABSTRACT

In order to better guide the design of industrial process for purification and recovery of VOCs, temperature swing adsorption (TSA) and temperature vacuum swing adsorption (TVSA) process for VOCs purification and recovery were studied systematically with activated carbon adsorbent. The adsorption and desorption behaviors of benzene on activated carbon in above two processes were investigated systematically. Effects of operating parameters on process performances were further analyzed, including as regeneration temperature, purging feed ratio and hot–cold purging ratio. The results showed that the increase of hot–cold purging ratio (HP/CP) could obtain the same regeneration effect as the increase of desorption temperature. Increasing the feed purge ratio without increasing the hot–cold purging ratio is not conducive to bed regeneration, because a large number of cold purge gases cannot utilize the residual heat of temperature wave, thus reducing the desorption effect of the cooling step on the bed. In addition, the vacuum step can enhance the regeneration ability of hot nitrogen to the bed at the same regeneration temperature, making the bed regeneration of TVSA process more thorough. Temperature in the middle and lower part of the bed in TVSA process was higher and the regeneration was more thorough. In conclusion, TVSA has more obvious advantages than TSA in terms of energy consumption, hot or cold purge volume and bed regeneration.

1. Introduction

Volatile organic compounds (VOCs) are the most common pollutants emitted by chemical, petrochemical, pharmaceutical and related industries [1,2], including benzene, toluene, xylene, chlorinated hydrocarbons, kerosene and so on [3,4]. Many volatile organic compounds have been detected to cause photochemical smog and haze in cities, and are even toxic to humans, causing health threats, such as sensory irritation symptoms, severe respiratory and metabolic disorders [5]. It was reported that China emitted about 23.3 million tons of volatile organic compounds into the atmosphere in 2015 [6]. Therefore, the removal and recovery of VOCs from tail gas has been paid more and more attention [7]. Many technologies for the treatment of tail gas containing volatile organic compounds have been proposed in the market, such as thermal oxidation, catalytic oxidation, adsorption, absorption, condensation, biofiltration and membrane technology [8]. At present, the most suitable control technology of volatile organic compounds is adsorption [9]. This method can be used to purify the tail gas or recover VOCs according to the different concentration of VOCs in the gas source. in the adsorption process, it is first adsorbed on the adsorbent, desorbed and then passed into the oxidation–reduction furnace or directly burned to complete the tail gas purification [10,11]. The desorbed VOCs gas can also be collected at the bottom of the bed, and the concentration can be increased to the extent that it can be recovered at room temperature or condensation to recover liquid VOCs [12,13]. Among them, Temperature swing adsorption is the mainstream technology for the treatment of VOCs [14–16]. There are many commercial adsorbents that can be used to control VOCs, including granular activated carbon (GAC), structured activated carbon, activated carbon fiber (ACF) and zeolite molecular sieves. It is true that it is easier to choose suitable adsorbents according to different molecular diameters and characteristics of VOCs, but activated carbon is still the most commonly used VOCs adsorbent [17]. The adsorption process is carried out in a cyclic manner. The airstream containing volatile organic compounds passes through the adsorbent bed, and the VOCs molecules are adsorbed in the adsorbent channel and the clean gas is released into the atmosphere. When the adsorption

* Corresponding author.
E-mail address: donghuizhang@tju.edu.cn (D. Zhang).

https://doi.org/10.1016/j.cjche.2022.01.029
1004-9541/

bed is saturated and it could not effectively capture VOCs. The duration of adsorption step should be terminated. The heat regeneration of adsorbent carried out subsequently and the VOCs would be desorption completely from adsorbent. After cooling adsorbent, a new cycle could start [17]. In industry, at least two adsorption beds are used alternately to complete the adsorption, heating and cooling steps to ensure continuous feeding [18]. After hot air purging and desorption, the activated carbon bed becomes hot and wet, and it is difficult to play a role in the adsorption step without going through drying and cooling steps [1,4,17,19]. Hot nitrogen purging does not need drying steps, however, a large flux of hot gas source is necessary to heat the bed directly by high temperature air flow, and the subsequent problem is that a large amount of purging gas dilutes the concentration of volatile organic compounds in the tail gas [18]. Therefore, a lower condensation temperature is often needed, and the price of nitrogen is very expensive, the amount of nitrogen and heating temperature have become issues worthy of discussion [20].

Nastaj *et al.* [21] studied the cyclic two-bed VTSA process of 2-propanol Sorbonorit 4 adsorption system on the basis of computer simulation. The effects of desorption temperature, pressure and the amount of purging gas on the desorption efficiency of 2-propanol were studied. the results show that compared with TSA process, the desorption process can be carried out with smaller purge flow under vacuum conditions, resulting in higher desorption component concentration, which can be recovered by condensation at medium temperature.

Using activated carbon as adsorbent, the dynamic simulation of cyclic thermal swing adsorption (TSA) system was carried out in Ko's study [22]. Through cyclic simulation, the effects of purge gas temperature on penetration curve, purge gas convergence time, cycle operation step, purge gas consumption, regeneration energy demand and purge gas adsorption capacity were discussed. The results show that the regeneration of the previous cycle does not completely affect the adsorption efficiency of the current cycle. When the regeneration temperature rises to a certain temperature point, the convergence rate of CSS will accelerate, but the further increase of regeneration temperature will cause the convergence rate of CSS to slow down.

Han *et al.* [23] studied the adsorption and desorption behavior of two typical polar-nonpolar VOCs (butyl acetate and *p*-xylene) on activated carbon by variable temperature-vacuum pressure swing adsorption (TS-VSA) process. Compared with single temperature swing adsorption (TSA) and vacuum pressure swing adsorption (VSA), this enrichment can not only significantly improve the desorption efficiency of total adsorbed VOC mixture (more than 30%), but also reduce desorption time and energy consumption. The results show that the removal and recovery of VOCs by activated carbon are stable and the adsorption capacity is more than 85%.

The theoretical and experimental study on the recovery of toluene (VOCs) from tail gas by activated carbon in circulating thermal swing adsorption (TSA) was carried out by Ambrożek [24]. The effects of purging gas and condensation temperature on the process efficiency were studied by computer simulation results. The results show that toluene can be recovered in the medium condensation temperature range even if the exhaust temperature is moderate [24].

Sui *et al.* [25] designed a set of pressure swing adsorption energy-saving device, which is used to remove high concentration toluene vapor from silica gel at room temperature. Vacuum desorption experiments show that at room temperature, the desorption rate of silica gel to toluene vapor (61.6%) is much higher than that of activated carbon (46.22%). At room temperature, the desorption rate of silica gel to toluene vapor is 61.6%, while that of activated carbon to toluene vapor is 46.22%. The adsorption of toluene by silica gel is easier and faster than that of activated carbon.

Jung *et al.* [26] investigated the effects of operating conditions such as benzene concentration, nitrogen flow rate, water vapor flow rate and bed temperature on the removal of VOC by TSA process. When the benzene concentration was 2% (vol), the total adsorption capacity of 13X zeolite and activated carbon was 4.44 g and 3.65 g, respectively. The results show that the desorption amount increases with the increase of bed temperature. However, when the temperature is above 150 °C, the desorption amount is basically unchanged and the energy consumption increases. The experiment of continuous cycle process showed that the amount of residual benzene at the end of regeneration remained basically unchanged after the fourth cycle.

Talmoudi *et al.* [27] uses activated carbon adsorption to recover dichloromethane and acetone from nitrogen. The effects of operating parameters such as adsorption step, vacuum and desorption temperature on the recovery of dichloromethane and acetone were investigated by establishing TSA/VSA adsorption model. The results show that TE vacuum pressure and desorption temperature should be carefully selected to reduce energy consumption and shorten the duration of purging steps. Hot nitrogen regeneration seems to be more effective than decompression regeneration.

Although there have been many theoretical and experimental studies on the TSA process [28–37], The purpose of this work was to systematically study the influence of operating variables on the process, especially the influence of hot and cold purging ratio and purge feed ratio on process recovery. At the same time, the desorption, cooling step temperature, concentration change trend, bed regeneration degree and their effects on the process were explored after adding vacuum steps, which was of practical significance to guide industrial design.

2. Process Description

2.1. TSA

In a typical TSA process, in order to meet the requirements of continuous feed in industry, the process in this study was designed as two beds. Table 1 provided the cycle sequence of the first stage of TSA process, including adsorption (AD), hot purge (HPUR) and cold purge (CPUR) steps. Fig. 1 showed a schematic diagram of the TSA loop. As shown in Fig. 1, the tail gas containing 0.4% (vol) C_6H_6 and 99.6% (vol) N_2 first passes through the adsorption bed (8000 s), the adsorption pressure was 101.325 kPa (or the exhaust pressure was selected), the strong adsorbate C_6H_6 was adsorbed on the activated carbon, and the weak adsorbate was discharged from the top of the bed. Before C_6H_6 penetrates the bed (the concentration of C_6H_6 at the top of the bed was lower than 10^{-7} or the emission standard was selected), the adsorption step was stopped to ensure that the exhaust gas met the emission standard. Then enter the hot purging step, the N_2 gas storage tank at the top of the bed introduces a stream of N_2 into the adsorption bed requiring hot purging and desorption (4000 s) after being heated by the heat exchanger at the top of the bed, with a large amount of C_6H_6 discharged from the bottom of the bed, when the temperature in the middle of the bed rised to 323 K, the desorption was stopped, and cold nitrogen was used to purge and cool down (4000 s). When the temperature of the exhaust gas from the bottom of the bed was lower than 320 K, the cooling step is stopped, the next cycle was started, and all steps were exactly the same as the first cycle.

Table 1
Cycle sequence of the TSA process

Time/s	4000	4000	4000	4000
BED A	AD	AD	HPUR	CPUR
BED B	HPUR	CPUR	AD	AD

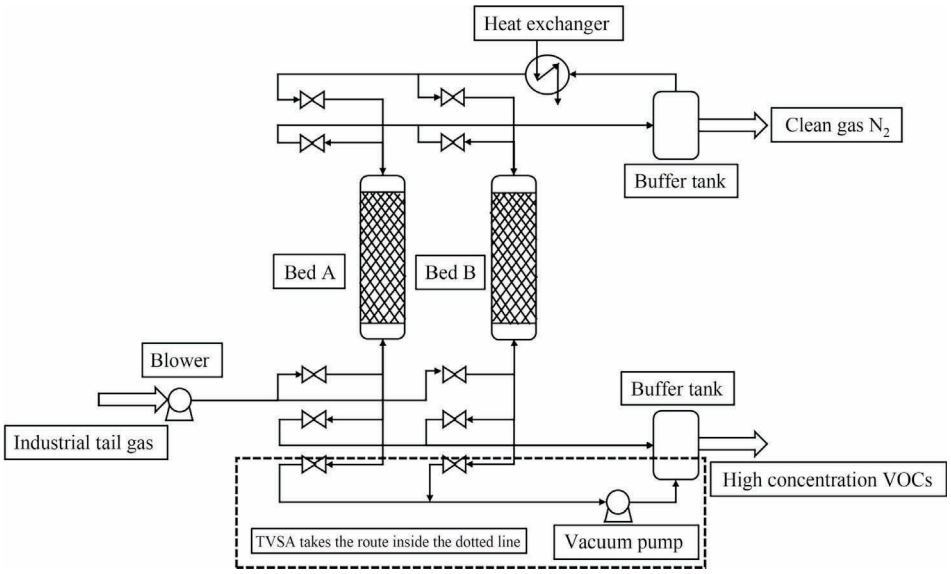

Fig. 1. Process schematic diagram for the TSA and TVSA cycle.

2.2. TVSA

The cycle structure and step sequence in the TVSA process were basically the same as those in the TSA process, except that the vacuum pump was added during hot purging and cold purging (the bed was gradually pumped to 0.03 MPa during hot purging, and the cold purging step vacuum pump provides the same power. The Cycle sequence is shown in Table 2.

3. Experiment and Mathematical Model

3.1. Dynamic adsorption experiment

Selecting an appropriate adsorbent is critical to the adsorption process. Activated carbon are the most commonly used adsorbents for purifying VOCs [7,22–24,28–31], Additionally, the activated carbon should be activated under vacuum at the temperature of 300 °C for 3 h before the applying to isotherm measurements. The adsorbates of high purity benzene (>99.999% (mass)) and N_2 (>99.999% (vol)) were supplied by Tianjin Taiya (Tianjin, China). The physical properties of the adsorbents are listed in Table 3.

Before the measurement of gas adsorption, the adsorbent sample was discharged under vacuum (10 kPa, absolute pressure) for 10 h at 450 K to remove impurities. In order to test the adsorption capacity of benzene on activated carbon, the adsorption isotherms of benzene on activated carbon were measured by high resolution Micromeritics3 Flex volumetric adsorption apparatus at five different temperatures (298 K, 348 K, 398 K, 448 K and 498 K). Using the device diagram was shown in Fig. 2, benzene vapor (4×10^{-3}) was dynamically adsorbed on activated carbon (see Fig. 3).

In this experiment, nitrogen was stored in a cylinder and used as an inert gas. Nitrogen was divided into two strands by a tee cock, both of which were controlled by a Flowmeter. One of the air streams produced benzene steam in the sealed container through continuous and stable bubbling, and the other air stream runs to dilute the benzene steam. The combined flow passes through the adsorption column (100 mm × 1000 mm), in which the adsorbent (3.14 g) was loaded. Another parallel bypass was designed to introduce benzene directly into the gas chromatography detector so that the initial concentration of benzene can be measured. Gas chromatography (GC7900, China Timi) was installed, equipped with a quartz capillary column (length × inner diameter × thickness, 50 m × 0.32 mm × 1.0 μm), a FID detector and a computer, and connected online to detect the airflow composition of the adsorption column. The temperatures of capillary column, detector and syringe were kept at 100 °C, 200 °C and 200 °C, respectively. Nitrogen and hydrogen were used as inert and fuel gases. Here, the initial concentration of benzene vapor was controlled at 4×10^{-3} by adjusting the needle valve. At room temperature, the velocity of the combined flow was fixed

Table 2
Cycle sequence of the TVSA process

Time/s	4000	4000	4000	4000
BED A	AD	AD	HPUR&VU	CPUR&VU
BED B	HPUR&VU	CPUR&VU	AD	AD

Table 3
Physical properties of Sorbonorit 4 activated carbon

Property	Value
Particle size/m	3.67×10^{-3}–7.2×10^{-3}
BET surface area/$m^2\cdot g^{-1}$	1200
Bulk density/$kg\cdot m^{-3}$	407
Heat capacity/$J\cdot kg^{-1}\cdot K^{-1}$	800

at 500 L·min^{-1} (101.325 kPa, 0 °C). For the desorption system, the heating vacuum desorption method was used to recover the adsorbed benzene from the saturated adsorbent. When the concentration of benzene vapor at the outlet was constant and close to or equal to the initial concentration, it was proved that the adsorbent is saturated by benzene vapor and reaches the adsorption equilibrium. Then, the adsorption column was removed and connected to the heating furnace and vacuum pump (498.15 K, 10 kPa, absolute pressure) to remove the adsorbed benzene. In the process of heating vacuum desorption, along with the heating and desorption of the heating furnace, and by changing the partial pressure of benzene vapor, inhaling air as desorption gas, further deep desorption of benzene (see Table 4).

3.2. Mathematical model [38]

In this section, we established a rigorous mathematical model to simulate TSA and TVSA processes reliably and accurately. The basic model of the adsorption process based on the laboratory scale was assumed as follows.

(1) The gas obeys the ideal gas law;
(2) Radial gradients of concentration, velocity and temperature are neglected;
(3) The gas phase and solid phase are in thermal equilibrium;
(4) Extended Langmuir model was employed to describe the competitive adsorption behaviors and the adsorption equilibrium;
(5) The pressure drop along the adsorption bed is described by the Eugen equation;
(6) The mass transfer between solid and gas phase are expressed by a linear driving force (LDF) model.

Based on the above assumptions, a mathematical model of mass, energy, momentum, and adsorption equilibrium was established to describe the dynamic adsorption behavior of C_6H_6 and N_2 in adsorption column.

The mass balance equation of component i based on the ideal gas assumption are expressed by Eq. (1):

$$-\varepsilon_b D a_{x,i}\frac{\partial^2 c_i}{\partial z^2}+\frac{\partial(v_g c_i)}{\partial z}+(\varepsilon_b+(1-\varepsilon_b)\varepsilon_p)\frac{\partial c_i}{\partial t}+\rho_s(1-\varepsilon_b)\frac{\partial q_i}{\partial_t}=0$$

$$\varepsilon_b\frac{\partial(v_g c)}{\partial z}+(\varepsilon_b+(1-\varepsilon_b)\varepsilon_p)\frac{\partial c}{\partial t}+\rho_s(1-\varepsilon_b)\sum_{i=1}^{n}\frac{\partial q_i}{\partial t}=0 \tag{1}$$

The axial dispersion coefficient $D_{ax,i}$ and D_m are calculated by Eq. (2) and Eq. (3) respectively:

$$D_{ax,i}=0.73D_{m,i}+\frac{v_g r_p}{\varepsilon_b(1+9.49\frac{\varepsilon_b D_{m,i}}{2v_g r_p})} \tag{2}$$

$$D_m=\frac{0.1013T^{1.75}\sqrt{(\frac{1}{M_A}+\frac{1}{M_B})}}{P(D_{v,A}^{1/3}+D_{v,B}^{1/3})^2} \tag{3}$$

Gas phase energy balance (Eq. (4)):

$$-k_g\varepsilon_b\frac{\partial^2 T_g}{\partial z^2}+C_{vg}v_g\rho_g\frac{\partial T_g}{\partial z}+\varepsilon_b C_{vg}\rho_g\frac{\partial T_g}{\partial t}+P\frac{\partial v_g}{\partial z}+h_f\alpha_p(T_g-T_s)+\frac{4h_w}{D_b}(T_g-T_0)=0 \tag{4}$$

Solid phase energy balance (Eq. (5)):

$$-k_s\frac{\partial^2 T_s}{\partial z^2}+C_{pw}\rho_w\frac{\partial Ts}{\partial t}+\rho_b\sum_{i=1}^{n}(C_{pa,i}w_i)\frac{\partial T_s}{\partial t}+\rho_b\sum_{i=1}^{n}\Delta H\frac{\partial q_i}{\partial t}-h_f\alpha_p(T_g-T_s)=0 \tag{5}$$

Adsorption bed wall energy balance (Eq. (6)):

$$-k_w\frac{\partial^2 T_w}{\partial z^2}+C_{pw}\rho_w\frac{\partial T_g}{\partial z}-h_w\frac{4D_b}{(D_b+W_t)^2-D_b^2}(T_g-T_w)+H_{amb}\frac{4(D_b+W_t)^2}{(D_b+W_t)^2-D_b^2}(T_w-T_{amb})=0 \tag{6}$$

The pressure drop along the adsorption bed is described by the Ergun equation given in Eq. (7):

$$-\frac{\partial P}{\partial z}=\frac{150\mu(1-\varepsilon_b)^2}{\varepsilon_b^3(2r_p\Psi)^2}v_g+1.75M\frac{(1-\varepsilon_b)\rho_g}{2r_p\Psi\varepsilon_b^3}|v_g|v_g \tag{7}$$

The extended Langmuir model is used to describe the competitive adsorption of C_6H_6 and N_2 on activated carbon is expressed by Eq. (8):

$$q_i^*=\frac{IP_{1i}e^{\frac{IP_{2i}}{T}}P_i}{1+\sum_{i=1}^{n}IP_3e^{\frac{IP_{4i}}{T}}P_i} \tag{8}$$

Finally, the linear driving force (LDF) model used to estimate lumped mass transfer rates is expressed by Eq. (9) [39,40]:

$$\frac{\partial q_i}{\partial t}=k_{LDK,i}(q_i^*-q_i) \tag{9}$$

While the mass transfer coefficient of component i is calculated by Eq. (10):

$$k_{LDF,i}=\frac{\Omega_c D_{c,i}}{r_c^2}=\frac{3D_{c,i}}{r_c^2} \tag{10}$$

In the above equation, the adsorption heat of the gas is calculated by the Clausius-Clapeyron equation (Eq. (11)):

$$-\Delta H_i=RT\left(\frac{\partial \ln P_i}{\partial T}\right) \tag{11}$$

The corresponding parameters and physical properties of the adsorbent as well as the adsorption bed are provided in Table 5. A series of parameters of feed and process operating are summarized in Table 6.

Additionally, three performance indicators include purity, recovery and energy consumption, which are employed to compare and evaluate the performance of various processes, as defined from Eq. (12) to Eq. (14).

$$\text{Purity}=\frac{\int_0^{t_{cycle}}F_{product}y_{product,i}dt}{\int_0^{t_{cycle}}F_{product}dt}\times 100\% \tag{12}$$

$$\text{Recovery}=\frac{\int_0^{t_{cycle}}F_{product,i}y_{product,i}dt}{\int_0^{t_{cycle}}F_{feed,i}y_{feed,c_6h_6}dt} \tag{13}$$

$$\text{Energy consumption}=\frac{\int_0^{t_{cycle}}\frac{F_{feed}P_{feed}\gamma}{\eta(\gamma-1)}\left[(\frac{P_{feed}}{P_{atm}})^{1-\frac{1}{\gamma}}-1\right]dt}{F_{product}}+\frac{\int_0^{t_{cycle}}\frac{F_{vac}P_{vac}\gamma}{\eta(\gamma-1)}\left[(\frac{P_{feed}}{P_{atm}})^{1-\frac{1}{\gamma}}-1\right]dt}{F_{product}}+S \tag{14}$$

for TSA and TVSA, S is the heating energy.

$$S=\frac{C_{pw}\rho_w V_{wall}(T_H-T_L)+C_{ps}\rho_s V_{col}(T_H-T_L)+\rho_b V_{col}\sum_{i=1}^{2}\Delta n_i(-\Delta H_i)}{F_{feed}t_{feed}} \tag{15}$$

Where Δn_i is the difference in loading on the heating stage.

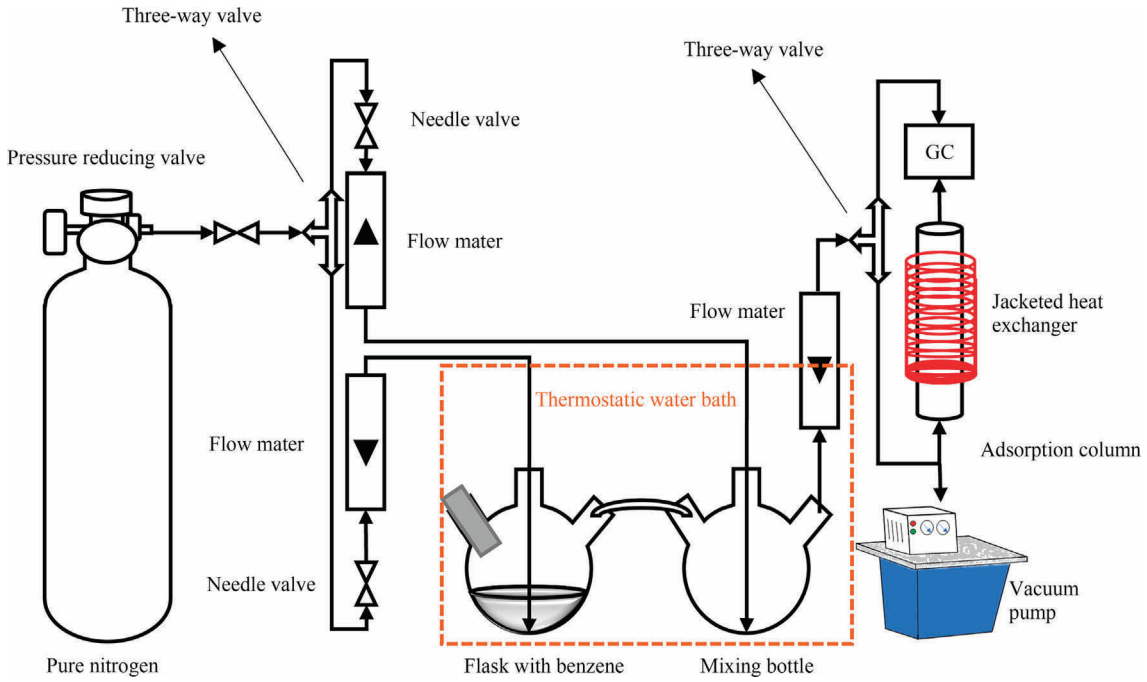

Fig. 2. Schematic diagram of experimental device.

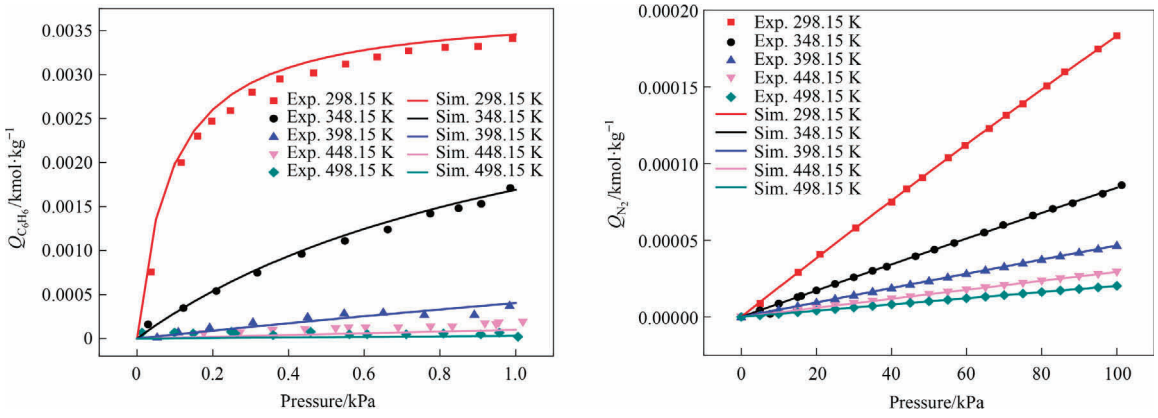

Fig. 3. Adsorption isotherms of C_6H_6 and N_2 on activated carbon.

Table 4
Adsorption isotherm parameters fitted by the extended Langmuir model

	IP1/kmol·kg^{-1}·kPa^{-1}	IP2/K	IP3/kPa^{-1}	IP4/K	ΔH/kJ·mol^{-1}
C_6H_6	2.85×10^{-9}	3471	4.18×10^{-4}	1570	−50.0
N_2	8.91×10^{-9}	1623	1.43×10^{-4}	351.3	−18.5

4. Results and Discussion

4.1. Analysis of the TSA process

The change of operation parameters will affect the performance of the whole process. Therefore, some key parameters, including feed flow rate, hot–cold purging ratio (HP/CP) and purge feed ratio (P/F), were selected to evaluate their effects on the performance of TSA. The corresponding simulation results were shown in Table 7.

It can be observed from Table 7 that with the increase of desorption temperature of 15%, the purity of nitrogen at the top of the bed increased from 99.901% (vol) to 99.996% (vol), the purity of C_6H_6 increases by 25% and the recovery increased by 21%. The reason was that the increase of desorption temperature made the bed regeneration more complete (Fig. 4(a)), the interception rate of C_6H_6 was higher and the purification effect was better in the adsorption step. Under the condition that the purge ratio was basically unchanged, the increase of C_6H_6 desorption amount will increase the purity and recovery of C_6H_6, and the energy consumption of treating each cubic meter of tail gas will also increase by 13%. Through run 4–6, it can be seen that when changing the HP/CP ratio (from 2.54 to 5.6), if the desorption temperature was not changed, it will not affect the maximum desorption concentration of C_6H_6, the purity of C_6H_6 or even the purity of N_2, but affected the recovery rate of C_6H_6. Because with the increase of the amount of hot nitrogen, although the desorption capacity of C_6H_6 increased

Table 5
Physical properties of adsorbent and adsorption bed

Parameters	Value
H_b/m	1
D/m	0.1
W_t/m	0.002
ε_b	0.44
ε_p	0.67
ψ	0.941
ρ_w/kg·m^{-3}	7800
C_{ps}/kJ·kg^{-1}·K^{-1}	0.8
C_{pw}/kJ·kg^{-1}·K^{-1}	0.52
$k_{LDF,C6H6}$/s^{-1}	1
$k_{LDF,N2}$/s^{-1}	0.5

Table 6
Parameters of feed and process operating conditions

Parameters	Value
Feed	
T/K	298.15
T_{amb}/K	298.15
P/MPa	0.1
Process operating conditions	
T_{cool}/K	298.15
T_{heat}/K	423.15

(Fig. 4(b)), and a large amount of hot nitrogen will dilute the desorption flow, which had a negative impact on the recovery of C_6H_6, but it had a real impact on the purification (higher bed regeneration), and the specific energy consumption increased by 30%. It can be seen that the higher the H/C purging ratio, was not the better, then there must be an optimal H/C purging ratio. This study was discussed in detail below. According to run 1, 8, 9, it can be seen that the increase of the ratio of P/F can significantly improve the purity of N_2 (purification effect). Due to the increase of the amount of N_2, the desorption purity of C_6H_6 is greatly diluted, although the recovery rate of C_6H_6 was improved, but a lower condensation temperature needed to recover C_6H_6. At the same time, the specific energy consumption increased greatly with the increase of C_6H_6 (75.9%). This showed that the bed can be further regenerated with the increase of P/F ratio (Fig. 4(c)). According to run 7, it can be found that reducing the feed rate can significantly improve the tail gas purification efficiency when other parameters in the process were limited, because the adsorption front was controlled in the bed (Fig. 5(a)). However, in order to maximize the process purification and recovery efficiency, other parameters need to be reasonably selected. Finally, according to run 3, 10, 11, it can be seen that the similar effect can be obtained by increasing the desorption temperature and increasing the hot and cold purging ratio. When using the adsorbent which was not resistant to high temperature, reducing the desorption temperature and increasing the H/C washing ratio can get a good effect. As shown in Fig. 5(b), the solid concentration curve at 453.15 K 15.3% (vol) purging ratio was lower than that of 483.15 K 12.2% (vol) purging ratio, indicating that increasing HP/CP can increase the desorption temperature. In addition, in order to prove that increasing purging ratio without increasing HP/CP ratio can not increase bed desorption rate, a group of control experiments (run 11) were carried out under the condition of 453.15 K 14.4% (vol) purging ratio. The solid concentration curve at the end of the desorption step should be between the black line and the green line, but the fact was that the purple line is higher than the black line, and the corresponding yellow line was higher than the green line, indicating that increasing the purging ratio without increasing the HP/CP ratio was not the main influencing factor. The reason was that although the amount of hot nitrogen purging increases after increasing the purging ratio, the amount of cold nitrogen is increased. The reason for the incomplete regeneration of the desorption step was that the heat provided by the increased hot purging was lower than that increased by increasing the regeneration temperature. although the amount of cold purging in the cooling step increases, but in the cold purging step, the regenerated bed essentially regenerates the bed by driving away the temperature wave in the bed, and excessive cold blowing will undoubtedly make the bed cool rapidly, resulting in a greater decrease in temperature during the process of temperature wave (Fig. 6). The adsorption bed cannot be further regenerated. On the contrary, after increasing the HP/CP ratio, we can see from Fig. 5(b) when the desorption step of 453.15 K 15.3% (vol) purging ratio ends the solid concentration curve (red line) was close to the solid concentration curve (green line) at the end of the cooling step. Finally, with the temperature wave is moved down by the cooling step to complete the complete desorption of the bed.

Fig. 6(a) showed that the gas temperature at the top of the bed is 360 K, the Fig. 6(b) was 380 K, and the highest Fig. 6(c) was 400 K, which verified the above conjecture that the intersection point of curve change on the way reflected the moving speed of the temperature wave. The greater the cold scavenging volume, the more to the right the intersection point. At the same time, this intersection point was also related to the temperature difference at

Table 7
Simulation results of TSA process with different operating conditions

Run No.	Feed flowrate /L·min^{-1} (101.325 kPa, 0 °C)	Com. /% (vol)	HP/CP /m^3·m^{-3}	P/F /kmol·kmol^{-1}	T/K	L/D	Max COD.	N_2 Pur. /% (vol)	C_6H_6 Pur. /% (vol)	C_6H_6 Rec /% (vol)	Energy consumption ratio/MJ·m^{-3}
	500	0.40	0.1325	3.75	423.15	10	0.0358	99.9010	2.07	78	0.0184
2	500	0.40	0.1274	3.75	453.15	10	0.0466	99.9720	2.42	82	0.0197
3	500	0.40	0.1220	3.75	483.15	10	0.0553	99.9960	2.58	85	0.0208
4	450	0.40	0.1294	2.54	423.15	10	0.0353	99.9104	2.16	80	0.0146
5	450	0.40	0.1473	3.75	423.15	10	0.0358	99.9611	2.07	80	0.0177
6	450	0.40	0.1464	5.60	423.15	10	0.0360	99.9700	2.17	80	0.0190
7	400	0.40	0.1657	3.75	423.15	10	0.0330	99.9999	1.96	90	0.0155
8	500	0.40	0.2651	3.75	423.15	10	0.0353	99.9975	1.19	88	0.0271
9	500	0.40	0.0835	3.75	423.15	10	0.0356	99.8206	2.36	73	0.0154
10	500	0.40	0.1532	5.00	453.15	10	0.0472	99.9970	2.07	85	0.0229
11	500	0.40	0.1442	3.20	453.15	10	0.04366	99.9401	2.15	83	0.0203

Note: Com.—component, COD.—Concentration of desorption.

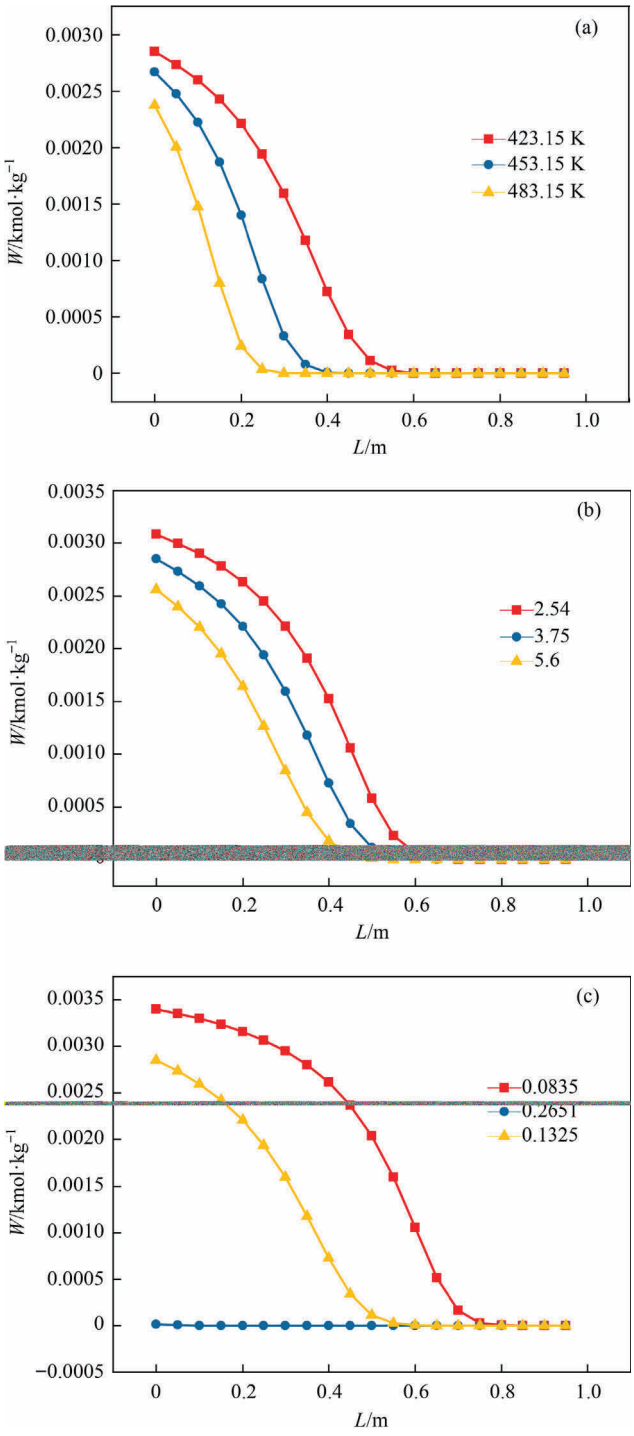

Fig. 4. The solid concentration distribution in the bed at the end of the desorption step. (a) Effect of different desorption temperature; (b) Effect of different hot and cold purging ratio; (c) Effect of different purge feed ratio.

the bottom of the bed (the intersection point moves to the right with the increase of the temperature difference), because the greater the temperature difference, the greater the slope of the uncooled part of the temperature curve. Because the preheating of the upper part of the bed will heat up the lower part of the bed, and the curve will shift to the lower left (the greater the amount of cold purge, the greater the downward range), so the intersection point moved to the right with the increase of temperature difference and to the left with the increase of cold purge. Finally, it can be determined that the greater the amount of cold blowing, the faster the cooling of the bed, the faster the point of intersection moves to the left, and the faster the regeneration of the bed, but the too fast temperature drop will also cause the waste heat of the temperature wave to be difficult to use effectively and weaken the effect of bed regeneration. The smaller the amount of blowing, the slower the cooling of the bed, in addition to causing the cooling of the bed not to completely affect the adsorption steps, it will also weaken the downward trend of the temperature curve and move to the left at the same time. Maximize the use of the waste heat of the temperature wave to help the bed desorption completely. All in all, the HP/CP ratio was an important parameter, and the appropriate HP/CP ratio can maximize the use of energy, desorption the bed to the maximum while making the bed cool perfectly, and avoid the heat loss caused by the high outlet temperature at the bottom of the bed in the thermal regeneration step.

4.2. The best HP/CP

We know that the main function of the hot nitrogen purge step and the cold nitrogen purge step was to control the bed temperature, the hot purge heats up to the desired desorption temperature, and the cold purge started the next cycle after cooling to the adsorption temperature. Secondly, the cold purge will make the temperature wave of the cooling step move downwards, and the further desorption of the bed can be realized by using this principle, and both hot and cold purging will affect the process. So what is the best ratio of hot nitrogen to cold nitrogen? In this study, the best blowing ratio of hot and cold nitrogen was determined by analyzing the relationship between HP/CP ratio and temperature difference, energy consumption and the relationship between C_6H_6 purity and regeneration degree. According to industrial experience, the total amount of purging is usually between 10% (vol)and 15% (vol), too low purge requires a higher temperature to complete bed regeneration, too high purge will consume too much nitrogen and reduce the economic benefits of the process, so the purge/feed ratio used in this study is 10% (vol) and 15% (vol). The simulation results are shown in Table 8.

First of all, the temperature difference, purity, recovery and specific energy consumption of 423.15 K and 483.15 K are compared(Fig. 7), when the temperature difference is greater than 3, the cooling efficiency of the bed was greatly reduced, and a lot of waste heat was wasted. At the same time, the energy consumption increases greatly, and the increasing trend of purity and recovery slowed down in varying degrees. The reason was that increasing the amount of hot purge in the desorption step will increase the desorption amount, however the increased amount of nitrogen at the same time will dilute the total desorption purity, and the slowing down of the increasing trend of recovery was that the further desorption of the bed can be completed by using the waste heat in the bed through the cold purge step, but with the increase of HP/CP ratio, the effect of the cooling step is greatly weakened with the decrease of the amount of cold purge (see Table 9).

Through the temperature, purity, recovery and specific energy consumption diagram of 15% (vol) purge feed ratio(Fig. 8), it can be further seen that the high HP/CP specific recovery decreased at 483.15 K. Despite the overall recovery rate is still rising, But this is due to the rise of desorption temperature so that the bed regeneration is complete and HP/CP ratio thoroughly improve at the same time. While increasing energy consumption, the bed regeneration of cooling step is weakened, also can see these phenomena in 423.15 K. All in all, the effect of the process was the best when the HP/CP ratio was 3, which can not only meet the requirements of bed heating and cooling, but also take into account purity, recovery and energy consumption. This effect was more obvious at high desorption temperature.

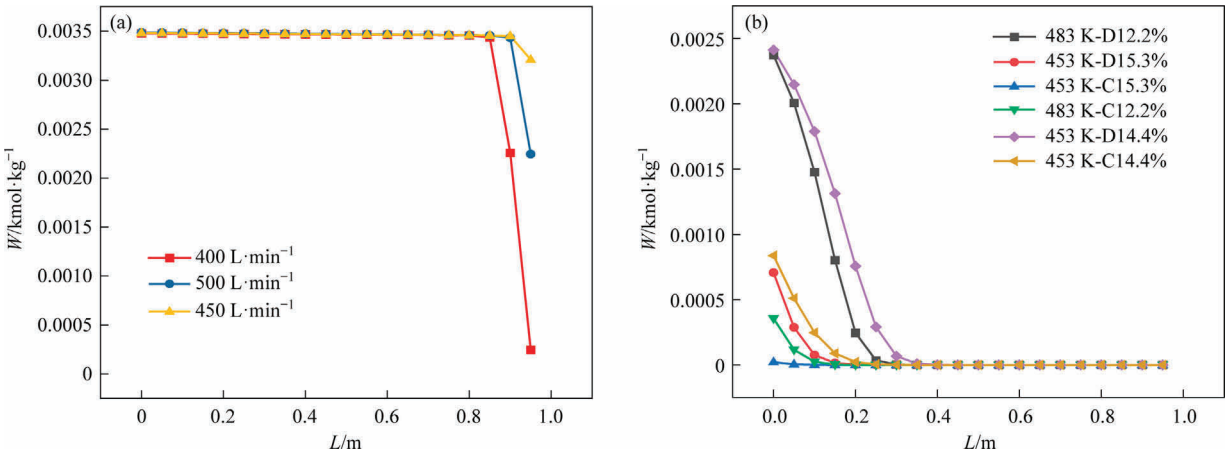

Fig. 5. (a) Adsorption fronts with different feed flowrate; (b) Influence of HP/CP ratio on solid concentration in hot and cold purge steps (D: End of desorption step, 12000 s; C: End of cool purging step, 16000 s).

4.3. Analysis of the TVSA process

From Fig. 9, we can clearly observe that The addition of vacuum steps leads to more complete bed regeneration. Fig. 9(a) can clearly display that the incomplete bed regeneration will cause the adsorption front of the next cycle to advance to the top of the bed, unable to complete the purification requirements, otherwise the treatment capacity will be sacrificed, while the bed desorption was more thorough after the hot purge and cold purge steps are vacuumed at the same time (Fig. 9(b)). At the end of the hot purge step, the bed is desorbed completely from 0.25 m to the top of the bed (only half of the bed can be desorbed in the vacuum-free step after the end of the desorption step). After the end of the cold purge step, part of the bed at the bottom of the bed is desorbed completely (in the vacuum-free step, 25% of the bed was not desorbed completely after the end of the cold purge step).

4.3.1. Effect of vacuum on desorption steps

As shown in Fig. 10, the coupling of vacuum steps had a significant effect on both hot and cold purge steps. first, the desorption step slows down the rise of bed temperature in the desorption step after adding the vacuum step, but caused the bed temperature to rise evenly, in addition, the vacuum step allowed the hot gas to pass through the bed faster, rather than heating from the top to the bottom of the bed, through Fig. 10(a) and (b). It was more intuitive to find the change of the red line, the temperature at the top of the bed is reduced by 10 K, but the temperature in the middle and lower part of the bed is obviously faster. Besides, in the middle of the bed (between 0.3 and 0.8 m), there was an obvious temperature fluctuation, which reflected that under the desorption of the hot purging gas at the top of the bed, the adsorbate in the gas phase is adsorbed in the middle of the bed where the temperature has not increased, and the secondary adsorption was formed. The addition of the vacuum step (Fig. 11(a)) makes the adsorbate not the same as the conventional step (Fig. 11(b)). The adsorbent has a strong adsorption exothermic phenomenon in the middle of the bed, so the temperature difference was small. The slow rising speed of the temperature in the vacuum step is that the secondary adsorption occurs successively from the middle of the bed to the bottom of the bed in the non-vacuum step, and the adsorption material in the vacuum step can not be lifted by the vacuum pump, and at the same time, the hot nitrogen passes through the bed faster.

In addition, the addition of the vacuum step makes the bed desorption faster in the hot purging step, and the adsorbate in the middle and lower part of the bed was removed from the adsorption bed before it was adsorbed. From the black box of Fig. 8, it can be found that the increase of adsorption capacity in the middle and lower part of the bed is significantly reduced. Combined with Fig. 12, it can be seen more intuitively that between 8000 and 8900 s, the adsorption capacity in the lower part of the vacuum step increased less, while the desorption capacity in the upper part of the bed is also significantly larger. Combined with Fig. 12, it can be found that a large number of adsorbents near the top of the bed are desorbed after adding the vacuum step, and the temperature changes from slow to rapid heating, while the bed temperature in the non-vacuum step rised rapidly and slowed down. the reason is that the desorption capacity of the bed becomes larger in the vacuum step, and the heat provided by hot nitrogen after complete desorption is completely used for bed heating, so the temperature rises faster.

4.3.2. Effect of vacuum step on cold purging step

Combined with Figs. 9 and 10, we found that the contribution of the cold purge step to the bed can be further desorbed by using the waste heat in the desorption step besides cooling the bed. According to Fig. 13(a), the vacuum step made the temperature front of the desorption step push downwards, and the temperature distribution in the middle and upper part of the bed is basically the same, with higher temperature in the middle and lower temperature at the bottom. As exhibited in Fig. 14(a), the solid concentration corresponding to the increase in temperature is lower, so it was the low solid concentration that caused the bed temperature to rise faster. As described in Fig. 13(b) and (c), we found that the higher temperature in vacuum occurs when there was no external heat source in the cold purging step, which was partly due to the higher bed temperature in the hot purging step, the other part was caused by the fact that the adsorbent was regenerated more thoroughly without endothermic desorption. Through Fig. 14(b) and (c), we can observe that the difference in solid con-

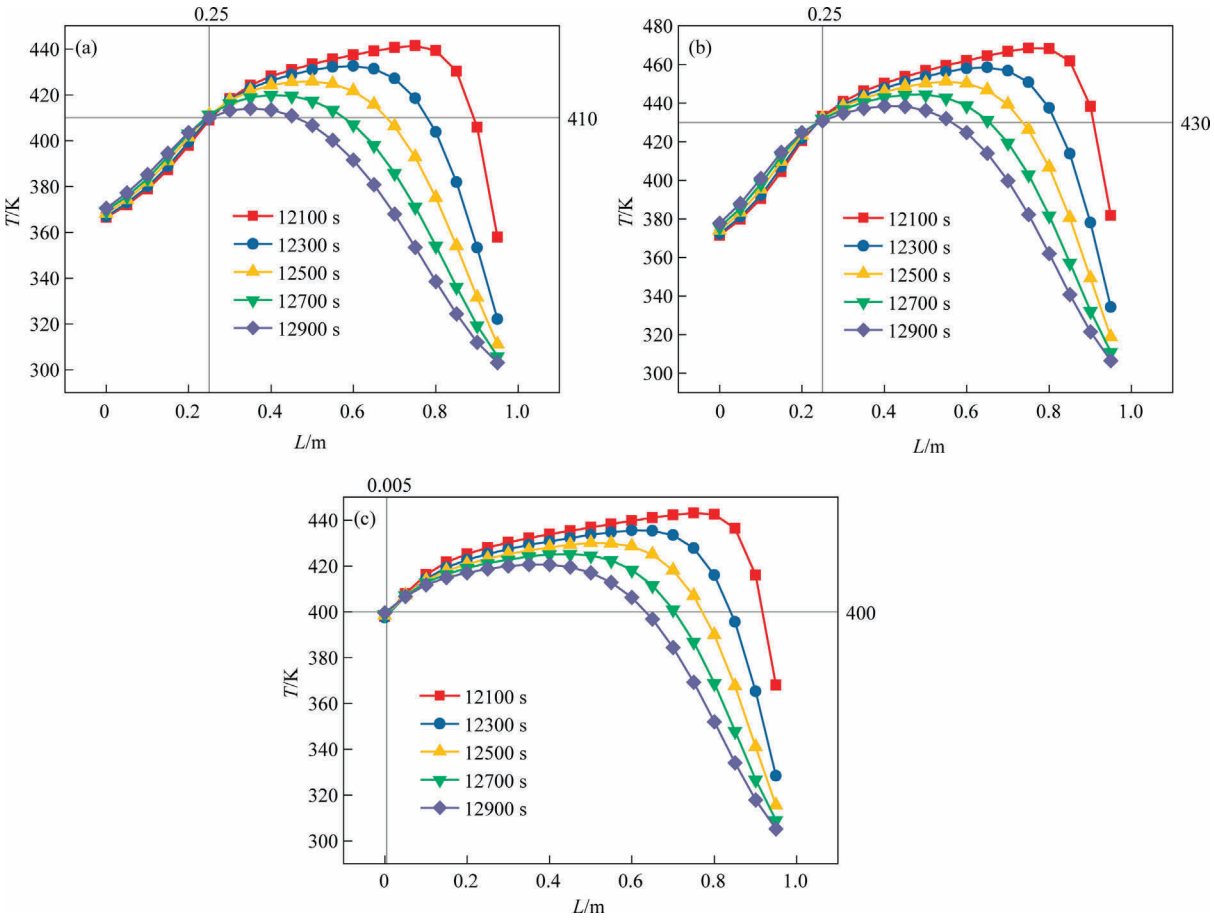

Fig. 6. The axial temperature trend of the bed within 1000 s after the cold purge. (a) T = 423.15 K, P/F = 14.4% (vol), HP/CP = 3.2; (b) T = 483.15 K, P/F = 12.2% (vol), HP/CP = 3.75; (c) T = 423.15 K, P/F = 15.3% (vol), HP/CP = 5.

Table 8
Simulation results of TSA process with different HP/CP

Run No.	T/K	HP/CP /$m^3 \cdot m^{-3}$	P/F /kmol·kmol^{-1}	L/D	T_{Outlet}/K	ΔT/K	Purity /% (vol)	Recovery /% (vol)	Energy consumption /MJ·m^{-3}
1	423.2	5	0.10	10	332	10	2.35	69.05	0.01702
2	423.2	4	0.10	10	328	13	2.27	71.34	0.01675
3	423.2	3	0.10	10	320	19	2.13	68.39	0.01634
4	423.2	2	0.10	10	312	20	1.88	64.61	0.01562
5	483.2	5	0.10	10	352	2	3.21	85.18	0.01899
6	483.2	4	0.10	10	349	2	3.10	85.39	0.01864
7	483.2	3	0.10	10	340	8	2.92	84.70	0.01811
8	483.2	2	0.10	10	324	26	2.58	82.68	0.01725
9	423.2	5	0.15	10	337	28	2.01	86.25	0.02051
10	423.2	4	0.15	10	328	35	1.93	85.53	0.02008
11	423.2	3	0.15	10	316	44	1.81	83.82	0.01948
12	423.2	2	0.15	10	305	50	1.59	79.84	0.01845
13	483.2	5	0.15	10	370	54	2.26	98.65	0.02344
14	483.2	4	0.15	10	352	69	2.18	98.66	0.02291
15	483.2	3	0.15	10	331	86	2.07	99.68	0.02213
16	483.2	2	0.15	10	310	63	1.94	98.72	0.02081

centration at the bottom of the bed is very significant. The temperature at the bottom of the bed was obviously higher without vacuum step, which showed that the rise of the temperature in the middle of the bed is mainly caused by the complete desorption of the bed and then the heating of the nitrogen heat source. Therefore, the vacuum step was added with a faster desorption speed, which in turn promotes the further desorption of the bed and improves the desorption efficiency. Finally, the cold purging step

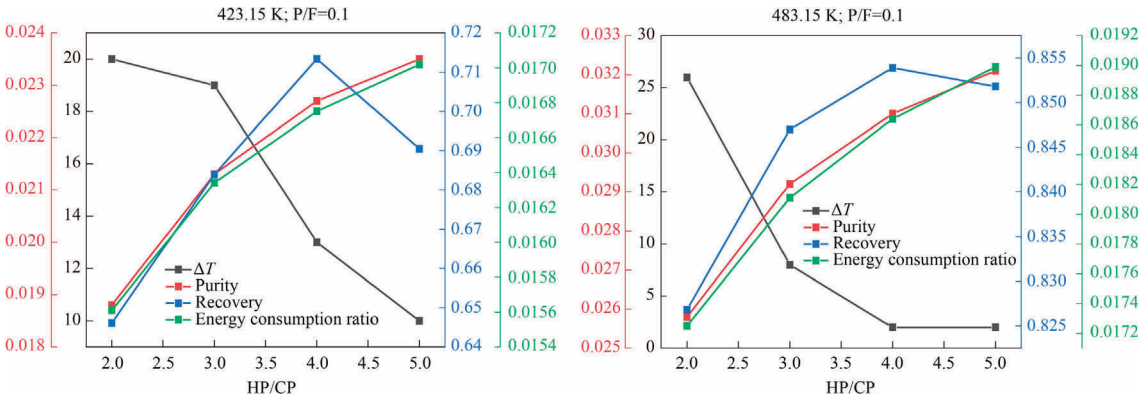

Fig. 7. The effect of different HP/CP on process. (At the same P/F and different regeneration temperatures).

Table 9
Comparison of process performance between TVSA and TSA

Run No.	Feed flowrate /L·min^{-1}	Com. /% (vol)	HP/CP /m^3·m^{-3}	Regeneration pressure/kPa	T/K	Max COD.	RE/% (vol)	Purge gas volume/m^3	Energy consumption ratio/MJ·m^{-3}
1	500	0.4	3.75	3	423.15	0.04488	96	25	0.0182
2	500	0.4	3.75	10	423.15	0.03577	75	25	0.0162
3	500	0.4	3.75	10	498.15	0.06377	97	25	0.0211
4	500	0.4	3.75	10	423.15	0.03642	100	40	0.0240

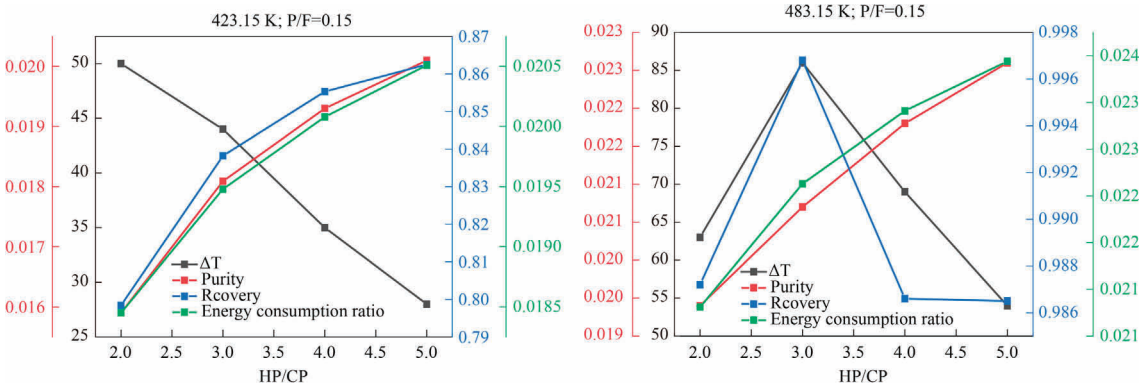

Fig. 8. The effect of different HP/CP on process. (At the same P/F and different regeneration temperatures).

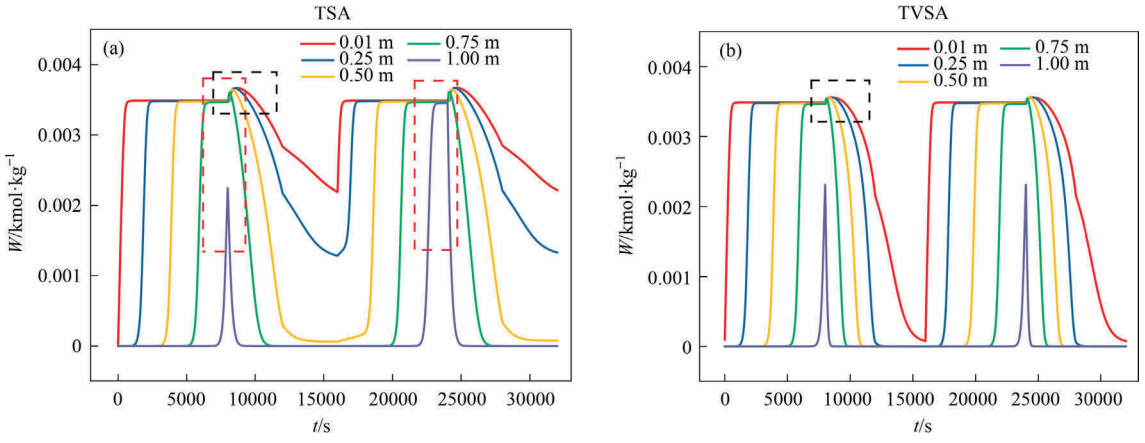

Fig. 9. Solid phase concentration curves of TSA and TVSA (a) T = 423.15 K, P = 0.1 MPa; (b) T = 423.15 K, P = 0.03 MPa. (The pressure under all vacuum conditions below is 3 kPa).

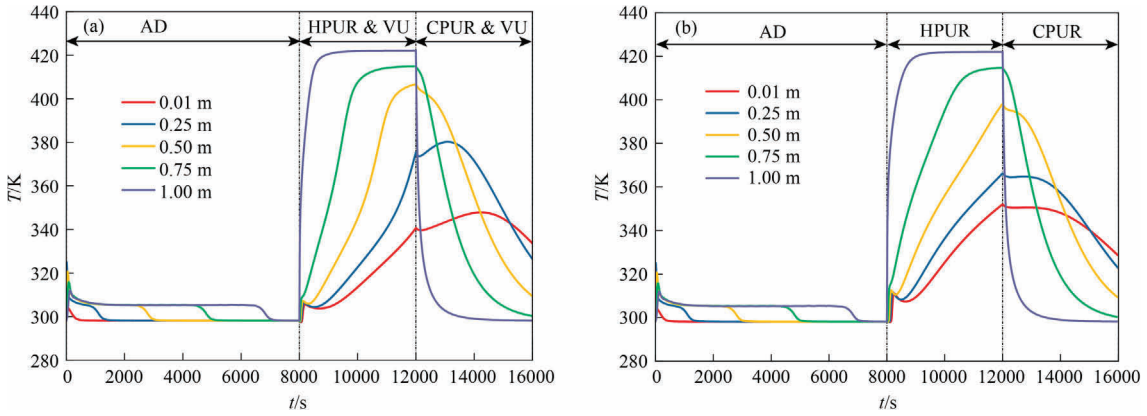

Fig. 10. The bed temperature curve of the whole process (a) TVSA; (b) TSA.

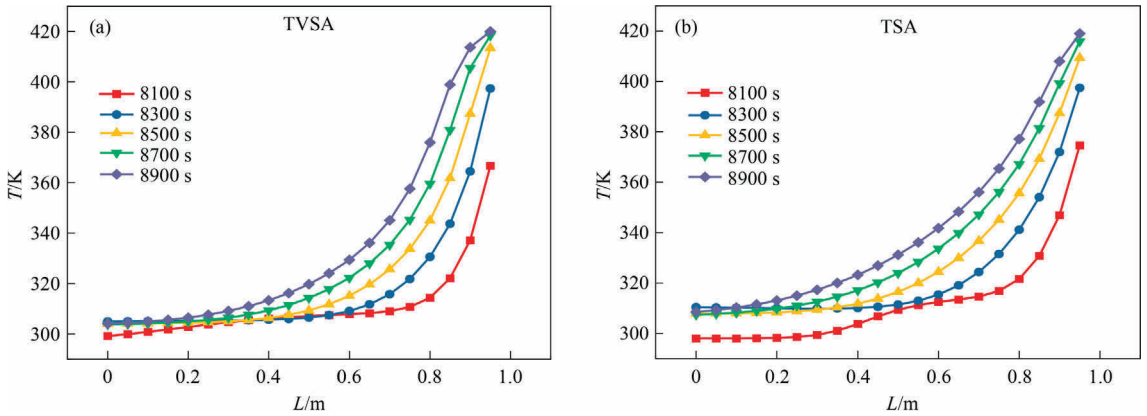

Fig. 11. The axial temperature curve of the bed during the first 1000 s at the beginning of the thermal regeneration step.

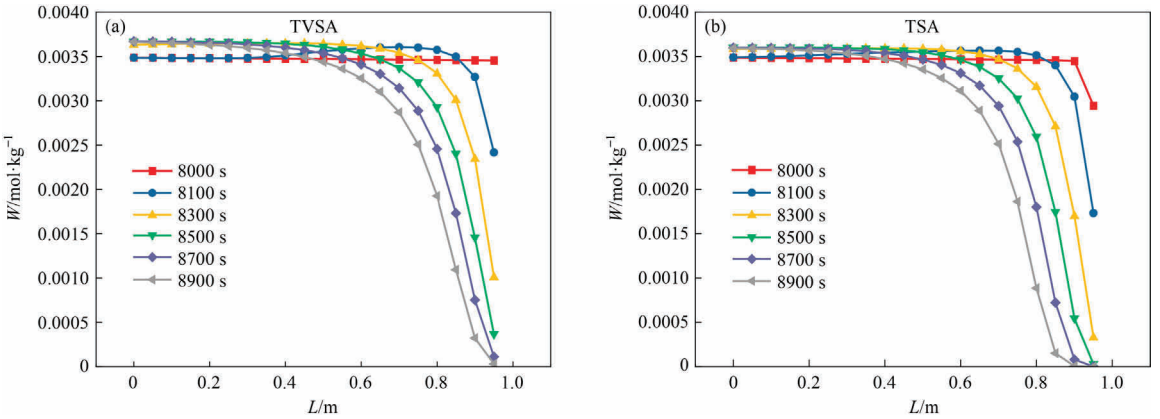

Fig. 12. Bed axis solid concentration curve 1000 s before the thermal regeneration step.

was of great significance to the bed regeneration. From Fig. 13(b) and (c), we can see that the cold purging step pushed the preheating of the bed from the top of the bed to the last bed at the bottom of the bed in the form of a temperature wave. Whether the bed temperature can be further increased in the cooling process depended on the amount of hot and cold scavenging, while the vacuum step can further increase the temperature in the middle of the bed under the same air volume ratio. The regeneration rate

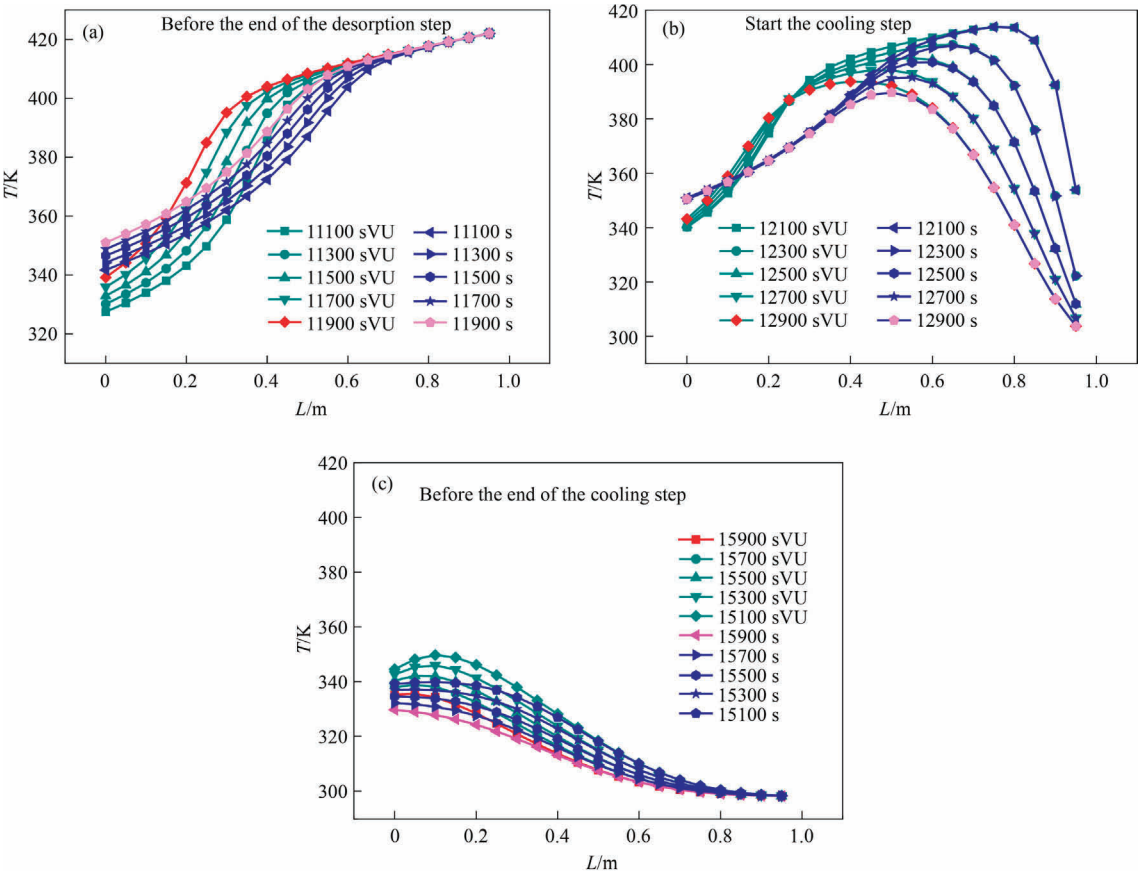

Fig. 13. Bed temperature curves of TVSA and TSA. (Dark green: P = 0.03 MPa; Deep blue: P = 0.1 MPa; pink: 100 seconds before the end of step in P = 0.1 MPa; red: 100 seconds before the end of step in P = 0.03 MPa).

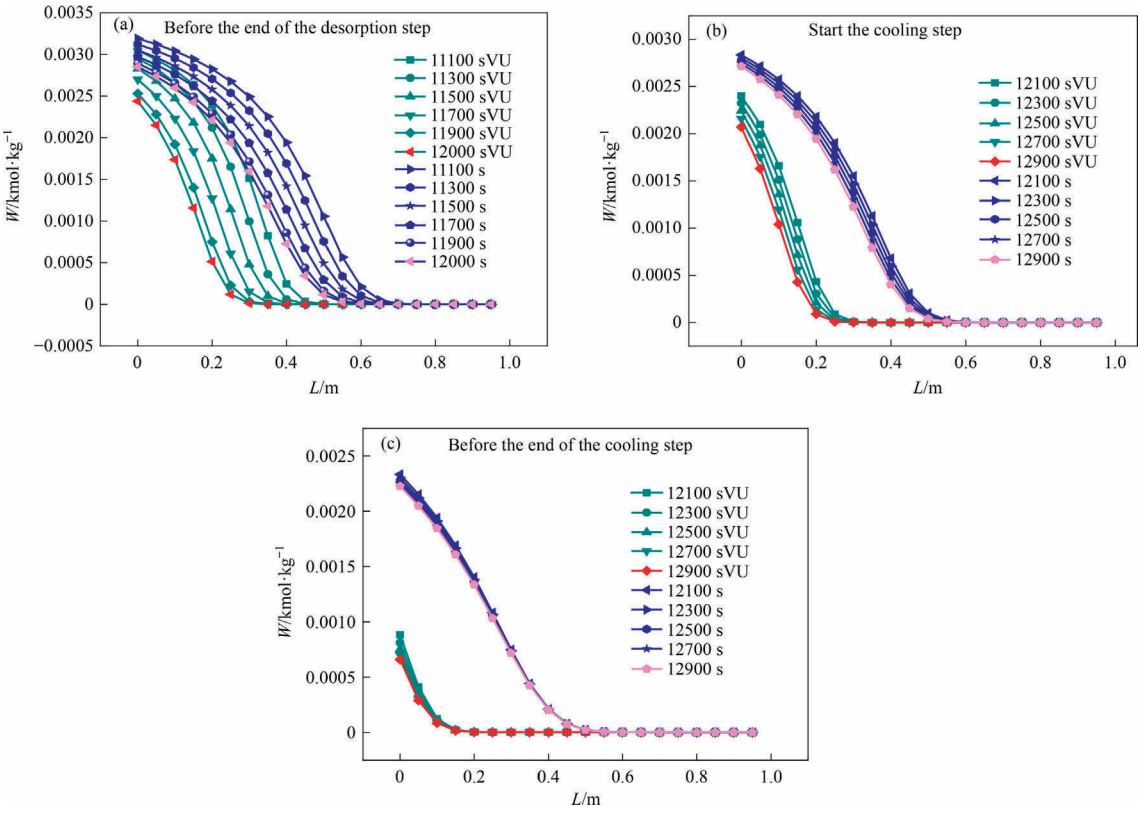

Fig. 14. Solid phase concentration curves of TVSA and TSA. (Dark green: P = 0.03 MPa; Deep blue: P = 0.1 MPa; pink: the end of step in P = 0.1 MPa; red: the end of step in P = 0.03 MPa).

of the bed was faster due to the vacuum step, so that more of the heat transferred from the top of the bed can be used to raise the temperature of the bed.

4.4. Performance comparison between TSA and TVSA

Combined with the above summary of the research on chemical engineering mass transfer and heat transfer process, the data of the above four cycles show that TVSA process has more advantages than TSA process. It not only reflects that the bed regeneration is higher under the same conditions, but also requires less purge gas. It can be seen from run 1,2 that TSA sacrifices the regeneration degree of the bed to reduce energy consumption at the same regeneration temperature, but this is obviously inconsistent with the industrial practice, while the energy consumption of TVSA decreases by 15.9% (vol) (run 1,3) under the condition of maintaining the same regeneration degree of the bed. The TVSA process reduces the amount of nitrogen required to complete bed regeneration by 60% (run 1,4) compared to the TSA process with increased purge gas, which will significantly reduce the volume of nitrogen tanks in industrial applications. Moreover, the reduced nitrogen purge will greatly increase the concentration of adsorbent in gas phase. Therefore, TVSA process has more advantages than TSA process in many aspects.

5. Conclusions

The process parameters of VOCs recovery in TSA and TVSA systems were studied by using the simulation results. Benzene was selected as adsorbent and activated carbon Sorbonorit 4 as adsorbent. These results showed that regeneration temperature, feed rate, purge feed ratio and hot–cold purging ratio all have influence on the process. Increasing regeneration temperature can promote bed desorption and increase hot–cold purging ratio can obtain similar effect. Simply increasing the purge feed ratio without increasing the hot blowing scavenging rate will not only reduce the purity of regenerated gas, but also have little effect on the bed regeneration, and even hinder the cold blowing step to use the temperature wave to desorb the bed. In addition, it was a reliable method to reduce the feed rate when other parameters cannot be changed, although there was still an adsorption saturation zone in the bed before the start of the bed regeneration and incomplete adsorption steps, however, reducing the feed rate can keep the adsorption front in the bed at the end of the adsorption step, and the tail gas treatment still has a purification effect. And finally there was an optimum ratio of hot and cold purging ratio. The lower the desorption temperature (the lower the purging rate), the closer to 4, and the higher the desorption temperature (the higher the purging rate), the closer to 2.5, so when designing the hot and cold purging ratio. The optimization should be more reasonable under the condition that the hot and cold purging gas volume at 3:1.

The TVSA process can improve the regeneration degree of the bed, in the desorption step, the hot purging gas can pass through the bed faster, the bed heating rate was faster and more uniform, and the desorption gas was removed from the bottom of the bed. In both TSA and TVSA processes, the concentration wave was faster than the temperature wave, but the addition of vacuum pump makes the concentration wave faster, shortens the mass transfer time, and weakens the secondary adsorption phenomenon and the temperature fluctuation in the middle and lower part of the bed. It not only reduced the heat loss, but also increased the heating rate of the bed, and then improved the regeneration degree of the bed. In addition, the vacuum step also had a significant effect on the cold purge step. In the TSA process, the cold purge step was usually the temperature wave faster than the concentration wave, but in TVSA, due to the influence of vacuum pump, the solid phase concentration wave in the bed was faster than the temperature wave, and the bed was desorbed first and then warmed up. As a result, the waste heat in the bed was used more efficiently in the cold purging step, and the heating effect of the middle and lower part of the bed was enhanced. At the same time, the enhancement of the heating effect of the bed promotes the further desorption of the bed.

The addition of vacuum step reduced the desorption temperature, which indicated that there was a suitable low-grade waste heat source. TVSA will be an energy-saving recovery VOCs process, the purification effect of a single time can reach more than 10 times under the concentration of 4×10^{-3}, and liquid VOCs can be condensed and recovered at room temperature through multiple purification processes. For TSA process, the effect of purification VOCs process is better than that of recovery process. But in the same bed regeneration degree requirements, TVSA is better than TSA in energy consumption, scavenging volume, bed regeneration and desorption concentration.

Declaration of Competing Interest

The authors declare that they have no known competing financial interests or personal relationships that could have appeared to influence the work reported in this paper.

Acknowledgements

The Renewable Energy and Hydrogen Projects in National Key Research and Development Plan of China (2019YFB1505002).

Nomenclature

A_{bed}	bed crossection area, m^2
a_{HX}	external specific surface area of heat exchanger, m^{-1}
b_i	adsorption affinity, kPa^{-1}
b_0	pre-exponential factor, kPa^{-1}
C_p	specific heat of gas phase mixture, $J\cdot mol^{-1}\cdot K^{-1}$
$C_{pa,i}$	specific heat of component i, $J\cdot mol^{-1}\cdot K^{-1}$
C_{ps}	specific heat of the adsorbent, $J\cdot kg^{-1}\cdot K^{-1}$
C_{pw}	specific heat of the bed wall, $J\cdot kg^{-1}\cdot K^{-1}$
C_{vg}	gas molar specific heat, $J\cdot kg^{-1}\cdot K^{-1}$
c_i	gas phase concentration of component i, $mol\cdot m^{-3}$
$D_{ax,i}$	axial dispersion coefficient of component i, $m^2\cdot s^{-1}$
D_b	bed diameter, m
$D_{b\text{-}1}$	bed diameter of first-stage, m
$D_{b\text{-}2}$	bed diameter of second-stage, m
$D_{m,i}$	molecular diffusion coefficient of component i, $m^2\cdot s^{-1}$
D_T	bed diameter of TSA and TVSA, m
H_{amb}	heat transfer coefficient between wall and ambient, $MW\cdot m^{-2}\cdot K^{-1}$
H_b	height of adsorbent layer, m
h_f	film heat transfer coefficient between gas and adsorbent, $W\cdot m^{-2}\cdot K^{-1}$
h_m	heat transfer coefficient between gas and bed wall, $W\cdot m^{-2}\cdot K^{-1}$
h_v	heat transfer coefficient between wall and fluid, $W\cdot m^{-2}\cdot K^{-1}$
k_g	gas phase heat conductivity, $W\cdot m^{-1}\cdot K^{-1}$
$k_{LDF,i}$	LDF coefficient, s^{-1}

k_s adsorbent thermal conductivity, $W \cdot m^{-1} \cdot K^{-1}$
k_w thermal conductivity of the bed wall, $W \cdot m^{-1} \cdot K^{-1}$
M_i molar mass of component i, $g \cdot mol^{-1}$
P pressure, kPa
q_i adsorbed phase concentration of component i, $mol \cdot kg^{-1}$
q_i^* adsorbed phase concentration in equilibrium with bulk component i, $mol \cdot kg^{-1}$
$q_{m,i}$ specific saturation adsorption capacity of component i, $mol \cdot kg^{-1}$
R_g ideal gas constant, $J \cdot mol^{-1} \cdot K^{-1}$
r_p adsorbent particle radius, m
T temperature, K
T_{amb} ambient temperature, K
T_{cool} cooling temperature, K
T_g gas phase temperature, K
T_H high temperature after heating, K
T_{heat} heating temperature, K
T_L low temperature before heating, K
T_s adsorbent temperature, K
T_w bed wall temperature, K
T_0 inner temperature of the wall, K
t time, s
U_{HX} over all heat transfer coefficient, $W \cdot m^{-2} \cdot K^{-1}$
u_0 superficial velocity, $m \cdot s^{-1}$
V standard volume flow rate, $m^3 \cdot h^{-1}$
V_{col} column volume, m^3
v_g velocity of the bulk gas, $m \cdot s^{-1}$
W_t wall thickness used of the bed, m
w_{ads} mass of the adsorbent, kg
z axial distance of the adsorption bed, m
α_{HX} external specific surface area of heat exchanger, $m^2 \cdot m^{-3}$
α_p specific particle surface area per unit volume of bed, $m^2 \cdot m^{-3}$
γ ratio of specific heats (C_p/C_v)
ε_b bed porosity
ε_p particle porosity
η compressor efficiency
μ bulk gas mixture viscosity, $kg \cdot m^{-1} \cdot s^{-1}$
ρ_b bulk solid density of adsorbent, $kg \cdot m^{-3}$
ρ_g gas phase density, $kg \cdot m^{-3}$
ρ_s adsorbent density, $kg \cdot m^{-3}$
ρ_w density of the column wall, $kg \cdot m^{-3}$
ψ shape factor of the adsorbent particle

References

[1] F.I. Khan, A. Kr Ghoshal, Removal of volatile organic compounds from polluted air, *J. Loss Prev. Process. Ind.* 13 (6) (2000) 527–545.
[2] S.H. Opperman, R.C. Brown, VOC emission control with polymeric adsorbents and microwave desorption, *Pollut Eng.* 31 (1) (1999) 58–60.
[3] T. Dobre, O.C. Pârvulescu, G. Iavorschi, M. Stroescu, A. Stoica, Volatile organic compounds removal from gas streams by adsorption onto activated carbon, *Ind. Eng. Chem. Res.* 53 (9) (2014) 3622–3628.
[4] A.K. Ghoshal, S.D. Manjare, Selection of appropriate adsorption technique for recovery of VOCs: an analysis, *J. Loss Prev. Process. Ind.* 15 (6) (2002) 413–421.
[5] J.A. Bernstein, N. Alexis, H. Bacchus, I.L. Bernstein, P. Fritz, E. Horner, N. Li, S. Mason, A. Nel, J. Oullette, K. Reijula, T. Reponen, J. Seltzer, A. Smith, S.M. Tarlo, The health effects of nonindustrial indoor air pollution, *J. Allergy Clin. Immunol.* 121 (3) (2008) 585–591.
[6] W. Wei, S. Wang, J. Hao, S. Cheng, Trends of chemical speciation profiles of anthropogenic volatile organic compounds emissions in China, 2005–2020, *Front. Env. Sci Eng.* 8 (1) (2014) 27–41.
[7] H. Sui, T. Zhang, J.X. Cui, X.Q. Li, J. Crittenden, X.G. Li, L. He, Novel off-gas treatment technology to remove volatile organic compounds with high concentration, *Ind. Eng. Chem. Res.* 55 (9) (2016) 2594–2603.
[8] E.C. Moretti, VOC control reduce VOC and HAP emissions, *Chem. Eng. Prog.* 98 (6) (2002) 30–40.
[9] H. Sui, J.J. Liu, L. He, X.G. Li, A. Jani, Adsorption and desorption of binary mixture of acetone and ethyl acetate on silica gel, *Chem. Eng. Sci.* 197 (2019) 185–194.
[10] E. Gabruś, D. Downarowicz, Anhydrous ethanol recovery from wet air in TSA systems - Equilibrium and column studies, *Chem. Eng. J.* 288 (2016) 321–331.
[11] G. Swetha, T. Gopi, S.C. Shekar, C. Ramakrishna, B. Saini, P.V.L. Rao, Combination of adsorption followed by ozone oxidation with pressure swing adsorption technology for the removal of VOCs from contaminated air streams, *Chem. Eng. Res. Des.* 117 (2017) 725–732.
[12] H. Zaitan, A. Korrir, T. Chafik, D. Bianchi, Evaluation of the potential of volatile organic compound (di-methyl benzene) removal using adsorption on natural minerals compared to commercial oxides, *J Hazard Mater* 262 (2013) 365–376.
[13] H. Zaitan, M.H. Manero, H. Valdés, Application of high silica zeolite ZSM-5 in a hybrid treatment process based on sequential adsorption and ozonation for VOCs elimination, *J. Environ. Sci. (China)* 41 (2016) 59–68.
[14] Y. Tavan, H. Azizpour, H. Bahmanyar, Mathematical modeling of volatile organic compounds removal over activated carbon, *J. Environ. Chem. Eng.* 9 (1) (2021) 104777.
[15] R. Dawson, A.I. Cooper, D.J. Adams, Chemical functionalization strategies for carbon dioxide capture in microporous organic polymers, *Polym. Int.* 62 (3) (2013) 345–352.
[16] H. Sui, P. Jiang, X. Li, J.J. Liu, X.G. Li, L. He, Binary adsorption equilibrium and breakthrough of *n*-butyl acetate and *p*-xylene on granular activated carbon, *Ind. Eng. Chem. Res.* 58 (19) (2019) 8279–8289.
[17] M. Breitbach, D. Bathen, Influence of ultrasound on adsorption processes, *Ultrason. Sonochem.* 8 (3) (2001) 277–283.
[18] D. Downarowicz, K. Ziętarska, Adsorption of propan-1-ol vapour on Sorbonorit 4 activated carbon–equilibrium and dynamic studies, *Pol. J. Chem. Technol.* 19 (4) (2017) 59–64.
[19] I. Smallwood, Solvent recovery handbook, Blackwell Science, Oxford, 2002.
[20] J. Nastaj, B. Ambrożek, Modeling of drying of gaseous mixtures in TSA system with fixed bed of solid desiccants, *Dry. Technol.* 30 (10) (2012) 1062–1071.
[21] J.F. Nastaj, B. Ambrożek, J. Rudnicka, Simulation studies of a vacuum and temperature swing adsorption process for the removal of VOC from waste air streams, *Int. Commun. Heat Mass Transf.* 33 (1) (2006) 80–86.
[22] D. Ko, M. Kim, I. Moon, D.K. Choi, Analysis of purge gas temperature in cyclic TSA process, *Chem. Eng. Sci.* 57 (1) (2002) 179–195.
[23] Z.W. Han, D. Wang, P. Jiang, H. Sui, L. He, X.G. Li, Enhanced removal and recovery of binary mixture of *n*-butyl acetate and *p*-xylene by temperature swing-Vacuum pressure swing hybrid adsorption process, *Process. Saf. Environ. Prot.* 135 (2020) 273–281.
[24] B. Ambrożek, K. Zwarycz-Makles, Theoretical and experimental studies of the recovery of volatile organic compounds from waste air streams in the thermal swing adsorption system with closed-loop regeneration of adsorbent, *Energy Convers. Manag.* 85 (2014) 646–654.
[25] H. Sui, H.X. Liu, P. An, L. He, X.G. Li, S. Cong, Application of silica gel in removing high concentrations toluene vapor by adsorption and desorption process, *J. Taiwan Inst. Chem. Eng.* 74 (2017) 218–224.
[26] M.-Y. Jung, S.-S. Suh, Effects of operating conditions on adsorption and desorption of benzene in TSA process using activated carbon and zeolite 13X, *Appl. Chem. Eng.* 29 (5) (2018) 594–603.
[27] R. Talmoudi, A. AbdelJaoued, M.H. Chahbani, Dynamic study of VSA and TSA processes for VOCs removal from air, *Int. J. Chem. Eng.* 2018 (2018) 2316827.
[28] R.Z. Wang, Z.Z. Xia, L.W. Wang, Z.S. Lu, S.L. Li, T.X. Li, J.Y. Wu, S. He, Heat transfer design in adsorption refrigeration systems for efficient use of low-grade thermal energy, *Energy* 36 (9) (2011) 5425–5439.
[29] F.B. Cortés, F. Chejne, J.M. Mejía, C.A. Londoño, Mathematical model of the sorption phenomenon of methanol in activated coal, *Energy Convers Manage.* 50 (2009) 1295–1303.
[30] T. Dobre, O.C. Pârvulescu, A. Jacquemet, V.A. Ion, Adsorption and thermal desorption of volatile organic compounds in a fixed bed–experimental and modeling, *Chem. Eng. Commun.* 203 (12) (2016) 1554–1561.
[31] B. Ambrożek, The simulation of cyclic thermal swing adsorption (TSA) process, Modelling Dynamics in Processes and Systems, Springer, Berlin, 2009.
[32] J.M. Schork, J.R. Fair, Parametric analysis of thermal regeneration of adsorption beds, *Ind. Eng. Chem. Res.* 27 (3) (1988) 457–469.
[33] C.C. Huang, J.R. Fair, Study of the adsorption and desorption of multiple adsorbates in a fixed bed, *AIChE J.* 34 (11) (1988) 1861–1877.
[34] J.H. Yun, D.K. Choi, H. Moon, Benzene adsorption and hot purge regeneration in activated carbon beds, *Chem. Eng. Sci.* 55 (23) (2000) 5857–5872.
[35] A. Jareteg, D. Maggiolo, H. Thunman, S. Sasic, H. Ström, Investigation of steam regeneration strategies for industrial-scale temperature-swing adsorption of benzene on activated carbon, *Chem. Eng. Process. Process. Intensif.* 167 (2021) 108546.
[36] T. Yamaguchi, K. Aoki, M. Sakurai, H. Kameyama, Adsorption and desorption of low-content toluene–ethyl acetate gas mixtures on fixed-bed activated carbon for removal and concentration by TSA, *KAGAKU KOGAKU RONBUNSHU* 40 (1) (2014) 18–26.

[37] P.K. Sharma, P.C. Wankat, Solvent recovery by steamless temperature swing carbon adsorption processes, *Ind. Eng. Chem. Res.* 49 (22) (2010) 11602–11613.
[38] wN. Jiang, Y.H. Shen, B. Liu, D.H. Zhang, Z.L. Tang, G.B. Li, B. Fu, CO_2 capture from dry flue gas by means of VPSA, TSA and TVSA, *J. CO_2 Util.* 35 (2020) 153–168.
[39] Y.H. Yang, Y.S. Chen, Z.F. Xu, L. Wang, P.K. Zhang, A three-bed six-step TSA cycle with heat carrier gas recycling and its model-based performance assessment for gas drying, *Sep. Purif. Technol.* 237 (2020) 116335.
[40] D. Ko, I. Moon, D.K. Choi, Analysis of the contact time in a cyclic thermal swing adsorption process, *Ind. Eng. Chem. Res.* 41 (6) (2002) 1603–1615.